Corrosion behavior of Hf0.5 Nb0.5 Ta0.5 Ti1.5 Zr refractory high-entropy in aqueous chloride solutions

Electrochemistry Communications 98 (2019) 63–68

Contents lists available at ScienceDirect

Electrochemistry Communications

journal homepage: www.elsevier.com/locate/elecom

Corrosion behavior of $Hf_{0.5}Nb_{0.5}Ta_{0.5}Ti_{1.5}Zr$ refractory high-entropy in aqueous chloride solutions

Qiongyu Zhou[a], Saad Sheikh[b], Ping Ou[d], Dongchu Chen[a], Qiang Hu[c,*], Sheng Guo[b,*]

[a] School of Materials Science and Energy Engineering, Foshan University, Foshan 528000, China
[b] Department of Industrial and Materials Science, Chalmers University of Technology, Gothenburg 41296, Sweden
[c] Institute of Applied Physics, Jiangxi Academy of Sciences, Nanchang 330029, China
[d] School of Materials Science and Engineering, Jiangxi University of Science and Technology, Ganzhou 341000, China

ARTICLE INFO

Keywords:
High-entropy alloys
Refractory alloys
Solid solution
Corrosion
Passivity

ABSTRACT

The $Hf_{0.5}Nb_{0.5}Ta_{0.5}Ti_{1.5}Zr$ refractory high-entropy alloy with excellent corrosion resistance in the 3.5 wt% NaCl solution is identified in this work. This refractory high-entropy alloy exhibits much better general corrosion resistance than that of the 316L stainless steel, due to its corrosion current density being about one fifth of that in the latter. Meanwhile, the pitting potential of $Hf_{0.5}Nb_{0.5}Ta_{0.5}Ti_{1.5}Zr$ reaches an unusually high value of +8.36 V, much higher than that of reported high-entropy alloys. The superior passivity of $Hf_{0.5}Nb_{0.5}Ta_{0.5}Ti_{1.5}Zr$ is accredited to the formation of a single-phase solid solution containing high amount of homogenously distributed passivity-promoting elements, and also the existence of metallic Ta and OH^- species in the passive film, which contribute to the high immunity to passive film breakdown.

1. Introduction

Corrosion is one of the most common failure modes of metals, and the cost due to corrosion of metals has been over 3% of the world's gross domestic product annually in recent years [1]. To alleviate the formidable challenge, corrosion control is considered as one of the strategic areas for metals-based civilization [2]. Generally, some metals or alloys would show inherently low corrosion rates due to the formation of passive films. However, the localized pitting, which rapidly leads to the failure of metals, cannot be avoided once the passive film breaks down [3]. Accordingly, design and fabrication of new alloys with high passivity, have drawn much attention of materials scientists and engineers [4].

High-entropy alloys (HEAs), which are composed of at least four principal metallic elements, are newly emerging metallic materials [5]. The alloying concept that is brought by HEAs, opens up an enormously large and unexplored compositional space. HEAs, depending on compositions, have exhibited many attractive properties in terms of hardness, strength, wear resistance, and resistance to high-temperature softening [6,7]. Besides, some HEAs have shown excellent corrosion resistance due to the claimed good passivation characteristics [8–10]. It is therefore quite intriguing to further explore the potential of HEAs, as novel metallic materials that could have high passivity.

As reported, the superior passivity of HEAs can be understood and explained based on their composition and structure. Usually, the HEAs with high corrosion resistance contains large amounts of passive elements such as group IVB elements (Ti, Zr, and Hf) and group VIB elements (Cr, Mo, and W), which facilitate the formation of stable barrier films [8–12]. Besides, the entropy stabilized single solid solution phase that is formed in HEAs can also contribute to preventing the pitting corrosion, which would preferably occur at the phase boundaries where the composition shows large variations [10]. However, to the best of our knowledge, pitting potential, E_{pit}, of known HEAs are no more than +3 V in the 3.5 wt% NaCl solution [9–18]. In other words, it remains to be a tremendous challenge to design novel alloys with high passivity. Here, we present a refractory HEA (RHEA) with surprisingly high E_{pit} in aqueous chloride solutions, which makes it a promising material to be used in extremely demanding and highly-sensitive service environments.

2. Experimental

The RHEA studied in this work, $Hf_{0.5}Nb_{0.5}Ta_{0.5}Ti_{1.5}Zr$, was developed in our previous work [7]. It was prepared by arc melting high purity (> 99.9%) elemental materials on a water-cooled copper plate in the Ar atmosphere. The ingots were flipped and re-melted five times for improved homogeneity. The final ingot has the dimension of about 66 mm (length) × 28 mm (width) × 10 mm (thickness). After

* Corresponding authors.
E-mail addresses: huq@jxas.ac.cn (Q. Hu), sheng.guo@chalmers.se (S. Guo).

https://doi.org/10.1016/j.elecom.2018.11.009
Received 22 October 2018; Received in revised form 14 November 2018; Accepted 15 November 2018
Available online 16 November 2018

solidification, the samples for experiments, with strictly the dimension of 10 mm × 10 mm × 1 mm, were prepared from the ingots by electrical discharge machining followed by grinding and polishing.

The microstructures and element distribution were investigated by back-scattering electron imaging (BSE), electron backscatter diffraction (EBSD) and energy disperse spectroscopy (EDS) using a field-emission scanning electron microscope (NOVA NanoSEM 230, FEI). The crystal structure was examined by an X-Ray diffractometer (XRD, Bruker D8 Advance) using the Cu K-alpha radiation (λ = 1.5406 Å), operating at 40 kV and 200 mA. Chemical compositions of the passive films formed on the HEA samples were analyzed by X-ray photoelectron spectroscopy (XPS, ESCALAB250XI, Thermo Fisher) using the Al K-alpha X-ray source (1486.6 eV).

The electrochemical measurements were performed using a Princeton PARSTAT4000A electrochemical workstation with a conventional three-electrode electrochemical cell, consisting of the HEA sample (with an exposed area of 1 cm^2), Pt sheet saturated-calomel electrode (SCE) as the working electrode, counter electrode, and reference electrode. Before tests, RHEA samples were epoxy encapsulated, polished, degreased in alcohol, washed in distilled water and dried in air. All tests were carried out in the 3.5 wt% NaCl solution (pH = 7 ± 0.2, open to air) at ambient temperature (25 °C). The potentiodynamic-polarization tests were performed at a scan rate of 1 mV/s from an initial potential of −1.3 V till the current density reached a maximum of 1 mA/cm^2. To confirm the data reproducibility, ten parallel $Hf_{0.5}Nb_{0.5}Ta_{0.5}Ti_{1.5}Zr$ RHEA samples were measured and the standard deviation of the E_{pit} was calculated. The EIS tests were carried out at open circuit potential with a sinusoidal potential amplitude of 10 mV, running from 100 kHz to 10 mHz. For comparison, 316L stainless steels (SS) and pure Ti (> 99.9%) were also tested under the same condition.

3. Results and discussion

According to the BSE image, inverse pole figure (IPF) map and the XRD pattern as shown in Fig. 1, the $Hf_{0.5}Nb_{0.5}Ta_{0.5}Ti_{1.5}Zr$ RHEA forms a single-phase bcc solid solution with equiaxed grains. It is noted that here that the microstructure looks different to the microstructure that was reported for the same material before [7,19], mainly because of the different cooling rate that was used here and in previous work. The average grain size of the $Hf_{0.5}Nb_{0.5}Ta_{0.5}Ti_{1.5}Zr$ RHEA is ~160 μm. In addition, EDS mapping of constituent elements in Figs. 1c–g shows that each element distributes quite homogeneously. Here in $Hf_{0.5}Nb_{0.5}Ta_{0.5}Ti_{1.5}Zr$, a single bcc solid solution with homogenously distributed passivating elements, is expected to possess a superior passive property.

As shown in the polarization curve in Fig. 2a, 316L SS exhibits a typical passivation behavior, and the extracted electrochemical parameters are quite analogous to previous studies [20]. For the $Hf_{0.5}Nb_{0.5}Ta_{0.5}Ti_{1.5}Zr$ RHEA, its corrosion current density (i_{corr}) is about one fifth of that of 316L SS, indicating that the general corrosion resistance of this RHEA is much better than that of 316L SS. In addition, the excellent corrosion resistance of the $Hf_{0.5}Nb_{0.5}Ta_{0.5}Ti_{1.5}Zr$ RHEA could be confirmed by its i_{corr} being quite close to that of pure Ti (Fig. 2a).

More strikingly, a highly significant passivation behavior, as characterized by the extremely noble E_{pit} of +8.36 V (standard deviation = 0.11), can be observed. The protective film is formed almost spontaneously at the corrosion potential (E_{corr}), based on the feature that the polarization curve changes directly into the passive region without a noticeable active to passive transition [11]. There exist two passive regions, with the first passive region (−0.1–1.47 V) showing a stable passive current density, whereas the second passive region (1.9–8.36 V) showing sporadic current fluctuations, due to the formation and re-passivation of metastable pits [21]. The current fluctuations occur sporadically and annihilate rapidly in this wide passive region, indicating a strong film repairing ability [22,23]. In the second passive region, the passive current densities (i_{pass}) of pure Ti increase gradually. By contrast, the i_{pass} of the $Hf_{0.5}Nb_{0.5}Ta_{0.5}Ti_{1.5}Zr$ RHEA is quite stable.

Fig. 2b–f show the Bode and Nyquist plots of the films formed on the RHEAs after passivation for 10 mins at the potentials within the passive region (specifically, 1.0 V, 1.9 V, and 5.0 V), and passivation for 3 mins at 8.5 V, respectively. Two electrical equivalent circuits in Fig. 2g (Q_{pass} and Q_{pit} are the constant phase element (CPE) for passive films without pits and containing pits/metastable pits, respectively; R_{pass} and R_{pit} are the polarization resistance depending on passive films without or with pits; R_{ct} is the charge-transfer resistance; R_s is the solution resistance) are used to fit the EIS spectra (Fig. 2g) [24,25]. As shown in the Bode plots (Fig. 2b), high and slanted impedance modulus values and the relatively stabilized phase angles (70–85°) at the medium-low frequencies for the samples passivated at the potentials within the passive region are observed, indicating a capacitive response which relates to the presence of the barrier passive films [26,27]. All the Nyquist plots (Fig. 2c–f) are characterized by an unfinished semi-circle, a feature which is potential dependent [27]. Meanwhile the values of impedance ($|Z|$) increase with the increase of passivation potentials (Fig. 2b), due to the increase of passive film thickness (δ, which could be compared by $1/Y_0$, here Y_0 is the proportionality factor for CPE impedance) and in the order of ($Y_{0\text{–}1.0v} > Y_{0\text{–}1.9v} > Y_{0\text{–}5.0v}$) [11]. In addition, R_{pass} or R_{pit} of the samples passivated at the potentials in the passive region are tremendously high ($R_{pass\text{-}1.0V} = 2.78 \times 10^{15}$, $R_{pass\text{-}1.9V} = 6.64 \times 10^{14}$, $R_{pit\text{-}5.0V} = 6.13 \times 10^{14}$ Ωcm^2, respectively), confirming that the formed passive films can act as semi-conductive barriers to anti-corrosion. By contrast, the sample passivated at 8.5 V shows a feature of passive breakdown, according to the characteristics of non-existent capacitive-like behavior (Fig. 2b), and the low R_{pit} value ($R_{pit\text{-}8.5V} = 2.97 \times 10^3$ Ωcm^2, shown in Fig. 2f).

To thoroughly understand these passivation behaviors, the passive films formed on the RHEAs were analyzed by XPS (Fig. 3). When the polarization tests run to the critical potentials within the passive region, the passive film is composed of a mixture of TiO_2, ZrO_2, HfO_2, Nb_2O_5, and Ta_2O_5 (Fig. 3b–f) [28,29]. All these species with stable chemical states have been demonstrated to benefit the formation of continuous, stable and protective passive films [8,28–30]. Meanwhile, OH^- species and metallic state Ta are also observed (Fig. 3a, d). The OH^- species, which may come from the hydrated metal oxides or adsorbed H_2O, can repair the passive film integrity and increase the resistance to the attack from chloride ions [28,31,32]. The metallic state Ta, a unique feature for the protective passive film formed on Ta alloys [8,33], has also been found on the surface of β type Ti–Ta–Hf–Zr alloys after polarization within the passive region [34]. By contrast, there exist no OH^- species and metallic Ta on the surface of samples after polarization to the transpassive region (8.5 V) (Fig. 3a). Instead, besides the highly charged and stable oxides species (TiO_2, ZrO_2, HfO_2, Nb_2O_5, Ta_2O_5), suboxide species such as Zr_2O_3, NbO_2, Ti_2O_3, Hf_2O_3, TaO_2 are detected in the destructed film (Fig. 3b–f) [8]. Ti_2O_3 is regarded as the inducement for the metastable pits [30]. Besides, suboxides such as Zr_2O_3, Hf_2O_3, NbO_2, and TaO_2 seen in the passive film are also regarded as un-protective oxides [8].

It seems that the existence of metallic Ta and OH^- species in the passive film could be responsible for the superior passivity of the $Hf_{0.5}Nb_{0.5}Ta_{0.5}Ti_{1.5}Zr$ RHEA. Furthermore, another factor should also be considered: the alloying concept of HEAs ensures that the high content of passivity-promoting elements is homogeneously distributed in the single-phase solid solution. Therefore, the compositional limit of added elements can be relaxed, so more passivity-promoting elements than in conventional alloys can be added. Besides, the preferential corrosion occurred in the phase boundaries or inhomogeneous compositions could be avoided, thanks to the formation of a homogeneous single-phase solid solution [10].

In summary, it can be concluded that a superior corrosion resistance is achieved in the $Hf_{0.5}Nb_{0.5}Ta_{0.5}Ti_{1.5}Zr$ RHEA, and is accredited to

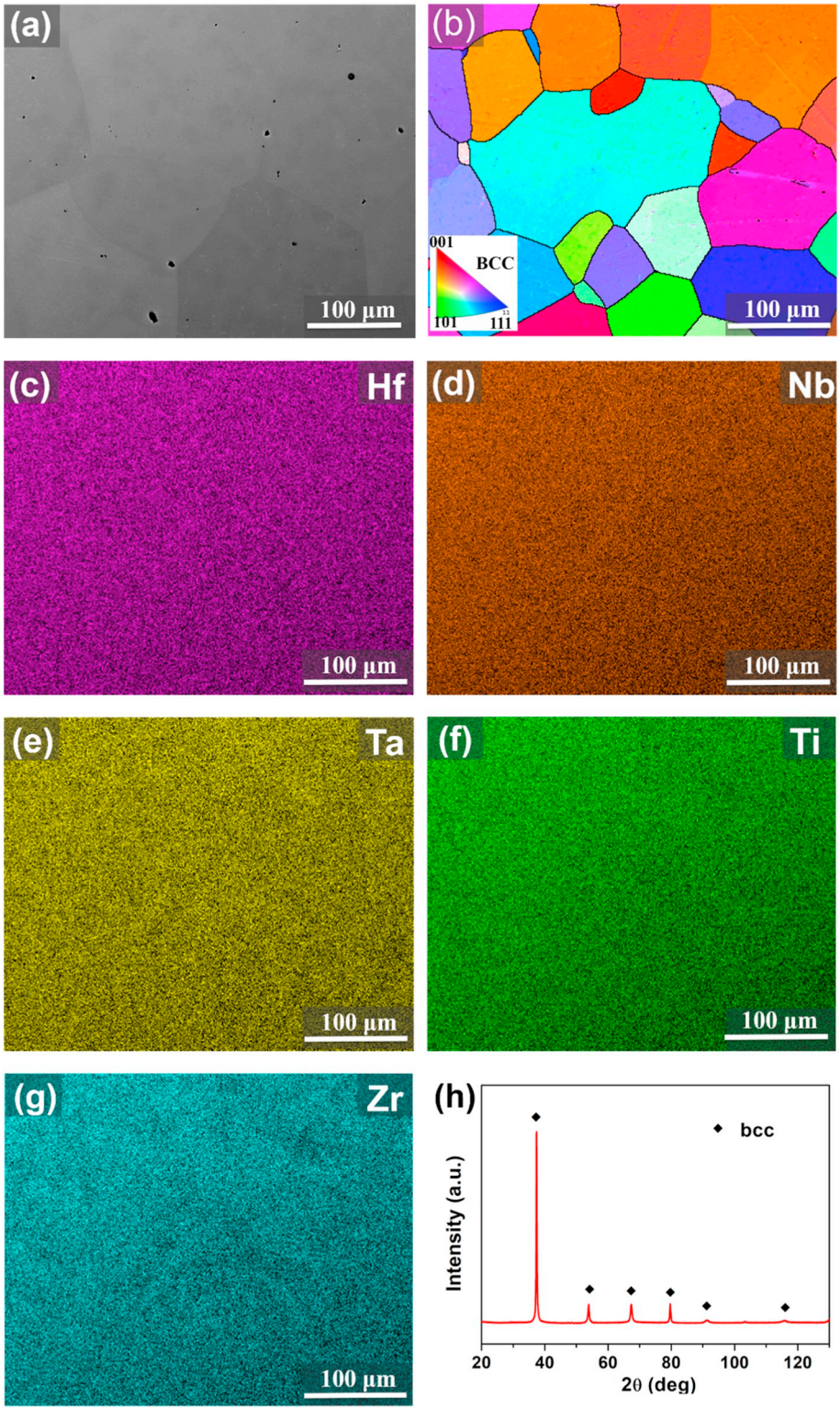

Fig. 1. a: BSE image, b: IPF map, c–g: EDS mapping and h: XRD pattern of the $Hf_{0.5}Nb_{0.5}Ta_{0.5}Ti_{1.5}Zr$ RHEA.

both the formation of a single-phase solid solution containing high amount of homogenously distributed passivity-promoting elements, and the high stability of the formed passive film. E_{pit} of the $Hf_{0.5}Nb_{0.5}Ta_{0.5}Ti_{1.5}Zr$ RHEA reaches an unusually noble value of +8.36 V. Nowadays, enormous efforts have been motivated to design new alloys to improve the resistance to localized corrosion. A detailed comparison of the corrosion behavior between the $Hf_{0.5}Nb_{0.5}Ta_{0.5}Ti_{1.5}Zr$ RHEA, and conventional passive alloys (Ni-, Ti-, Cu-, Al-based alloys and stainless steels) and other reported HEAs in the 3.5 wt% NaCl solution is plotted in Fig. 4 [9–18,20,35,36]. As shown in Fig. 4, some HEAs already exhibit higher E_{pit} than that of conventional passive alloys. Particularly, the $Hf_{0.5}Nb_{0.5}Ta_{0.5}Ti_{1.5}Zr$ RHEA that is studied here, exhibits the highest E_{pit} among all reported HEAs, showcasing the tremendous possibility of RHEAs for future applications, such as seawater desalination, naval armament, and chemical vessels.

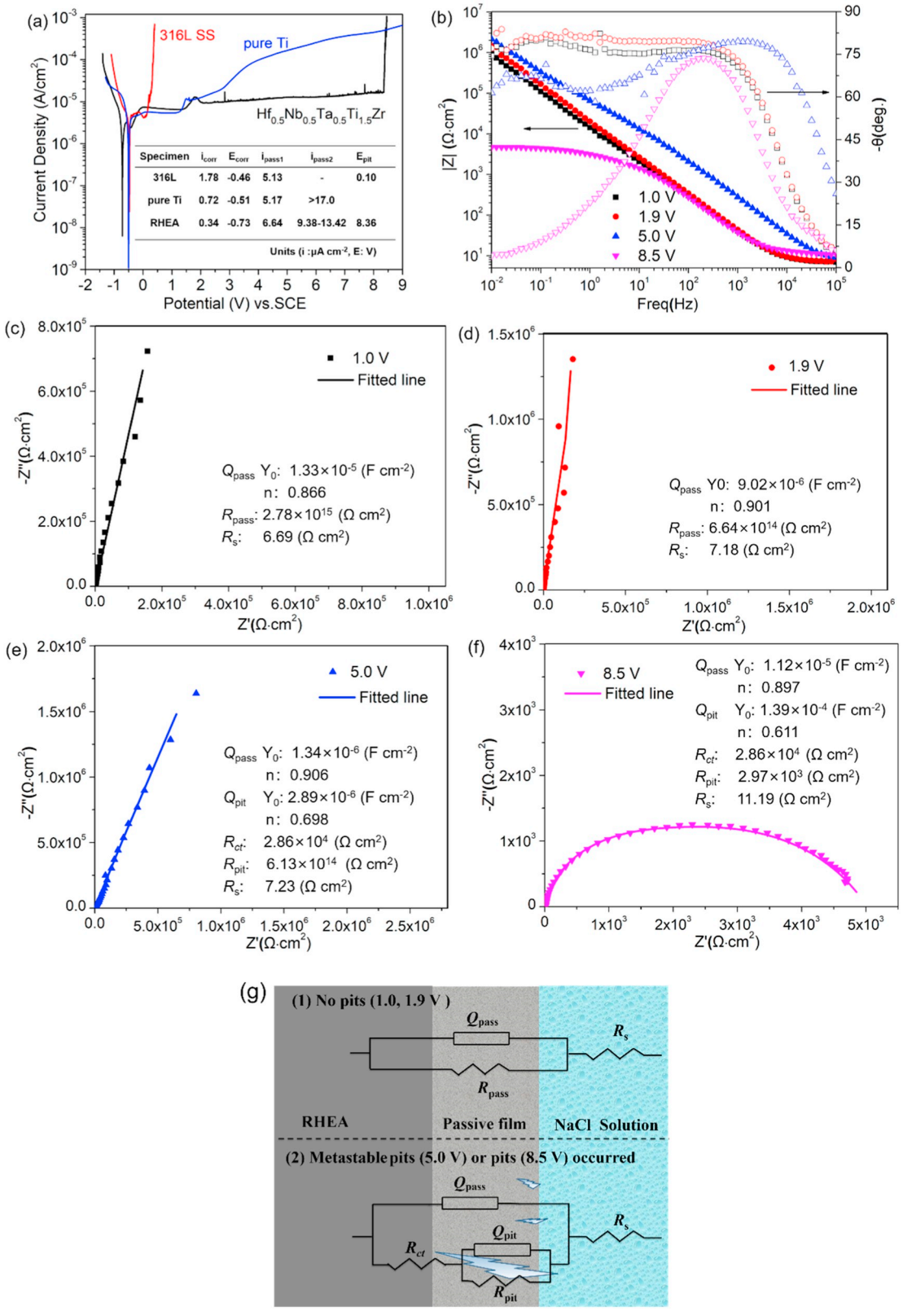

Fig. 2. a: Polarization curves of the $Hf_{0.5}Nb_{0.5}Ta_{0.5}Ti_{1.5}Zr$ RHEA, 316L SS and pure Ti in the 3.5 wt% NaCl solution, b–f: Nyquist and Bode plots of the $Hf_{0.5}Nb_{0.5}Ta_{0.5}Ti_{1.5}Zr$ RHEA in the 3.5 wt% NaCl solution, g: Equivalent electrical circuit for fitting the EIS experimental data.

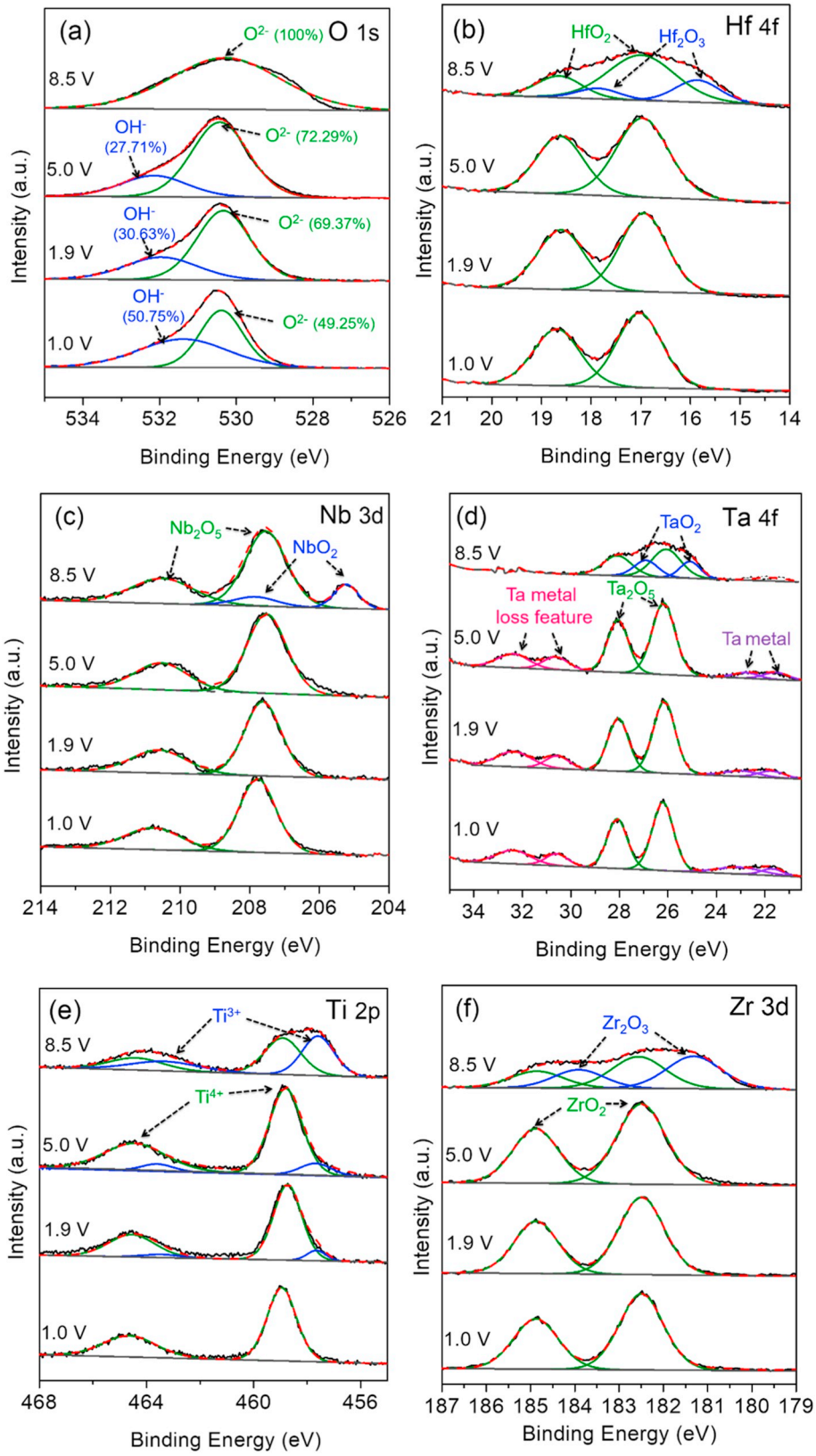

Fig. 3. XPS spectra made at the outer surface of samples after polarization ran to the chosen potentials.

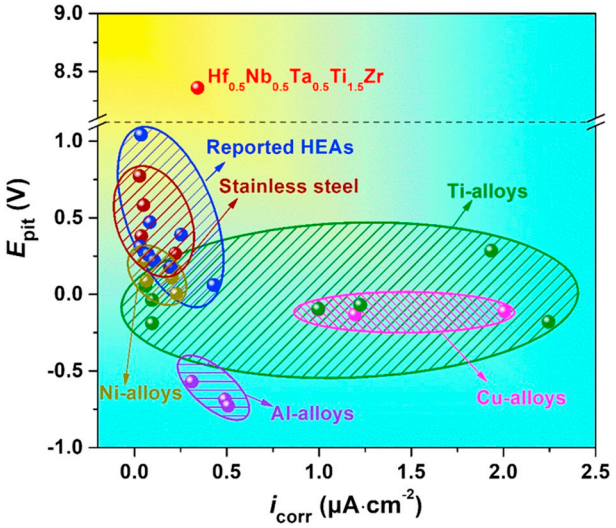

Fig. 4. Comparison of E_{pit} and i_{corr} for the $Hf_{0.5}Nb_{0.5}Ta_{0.5}Ti_{1.5}Zr$ RHEA, previously reported HEAs, and some conventional passive alloys in the 3.5 wt% NaCl solution.

4. Conclusion

The corrosion resistance of the $Hf_{0.5}Nb_{0.5}Ta_{0.5}Ti_{1.5}Zr$ RHEA in the 3.5 wt% NaCl solution is investigated in this work. This RHEA exhibits much better general corrosion resistance than that of 316L SS, due to its much lower corrosion current density. Meanwhile, an unusually noble E_{pit} of +8.36 V for the $Hf_{0.5}Nb_{0.5}Ta_{0.5}Ti_{1.5}Zr$ RHEA is revealed. The superior passivity is mainly attributed to the formation of a single-phase solid solution containing high amount of homogenously distributed passivity-promoting elements (Hf, Nb, Ta, Ti and Zr), and the existence of metallic Ta and OH^- species in the passive film. The work presented here exemplifies that the alloying strategy of HEAs could be an important future research direction, to meet the global challenge of corrosion control.

Acknowledgements

This work is supported by the National Natural Science Foundation of China (51504104), Natural Science Foundation of Jiangxi Province, China (20161BAB206141). SS and SG are grateful for the financial support from Areas of Advance Materials Science from Chalmers University of Technology.

References

[1] S. Ding, T. Xiang, C. Li, S. Zheng, J. Wang, M. Zhang, C. Dong, W. Chan, Fabrication of self-cleaning super-hydrophobic nickel/graphene hybrid film with improved corrosion resistance on mild steel, Mater. Des. 117 (2017) 280–288.
[2] A. Poursaee, Temperature dependence of the formation of the passivation layer on carbon steel in high alkaline environment of concrete pore solution, Electrochem. Commun. 73 (2016) 24–28.
[3] P. Schmuki, From Bacon to barriers: a review on the passivity of metals and alloys, J. Solid State Electrochem. 6 (2002) 145–164.
[4] S.S. Jamali, S.E. Moulton, D.E. Tallman, Y. Zhao, J. Weber, G.G. Wallace, Self-healing characteristic of praseodymium conversion coating on AZNd mg alloy studied by scanning electrochemical microscopy, Electrochem. Commun. 76 (2017) 6–9.
[5] J.W. Yeh, S.K. Chen, S.J. Lin, J.Y. Gan, T.S. Chin, T.T. Shun, C.H. Tsau, S.Y. Chang, Nanostructured high-entropy alloys with multiple principal elements: novel alloy design concepts and outcomes, Adv. Eng. Mater. 6 (5) (2004) 299–303.
[6] D.B. Miracle, O.N. Senkov, A critical review of high entropy alloys and related concepts, Acta Mater. 122 (2017) 448–511.
[7] S. Sheikh, S. Shafeie, Q. Hu, J. Ahlström, C. Persson, J. Veselý, J. Zýka, U. Klement, S. Guo, Alloy design for intrinsically ductile refractory high-entropy alloys, J. Appl. Phys. 120 (2016) 164902.
[8] J. Jayaraj, C. Thinaharan, S. Ningshen, C. Mallika, U.K. Mudali, Corrosion behavior and surface film characterization of TaNbHfZrTi high entropy alloy in aggressive nitric acid medium, Intermetallics 89 (2017) 123–132.
[9] Y. Qiu, S. Thomas, M.A. Gibson, H.L. Fraser, N. Birbilis, Corrosion of high entropy alloys, npj Materials Degradation 1 (2017) 15.
[10] Y. Shi, B. Yang, P.K. Liaw, Corrosion-resistant high-entropy alloys: a review, Meta 7 (2017) 43.
[11] Y. Shi, B. Yang, X. Xie, J. Brechtl, K.A. Dahmen, P.K. Liaw, Corrosion of $Al_xCoCrFeNi$ high-entropy alloys: Al-content and potential scan-rate dependent pitting behavior, Corros. Sci. 119 (2017) 33–45.
[12] C.M. Lin, H.L. Tsai, Evolution of microstructure, hardness, and corrosion properties of high-entropy $Al_{0.5}CoCrFeNi$ alloy, Intermetallics 19 (2011) 288–294.
[13] Y.J. Hsu, W.C. Chiang, J.K. Wu, Corrosion behavior of $FeCoNiCrCu_x$ high-entropy alloys in 3.5% sodium chloride solution, Mater. Chem. Phys. 92 (2005) 112–117.
[14] C.L. Wu, S. Zhang, C.H. Zhang, H. Zhang, S.Y. Dong, Phase evolution and cavitation erosion-corrosion behavior of $FeCoCrAlNiTi_x$ high entropy alloy coatings on 304 stainless steel by laser surface alloying, J. Alloys Compd. 698 (2017) 761–770.
[15] S. Zhang, C.L. Wu, C.H. Zhang, M. Guan, J.Z. Tan, Laser surface alloying of FeCoCrAlNi high-entropy alloy on 304 stainless steel to enhance corrosion and cavitation erosion resistance, Opt. Laser Technol. 84 (2016) 23–31.
[16] C. Shang, E. Axinte, J. Sun, X. Li, P. Li, J. Du, P. Qiao, Y. Wang, CoCrFeNi $(W_{1-x}Mo_x)$ high-entropy alloy coatings with excellent mechanical properties and corrosion resistance prepared by mechanical alloying and hot pressing sintering, Mater. Des. 117 (2017) 193–202.
[17] Q. Ye, K. Feng, Z. Li, F. Lu, R. Li, J. Huang, Y. Wu, Microstructure and corrosion properties of CrMnFeCoNi high entropy alloy coating, Appl. Surf. Sci. 396 (2017) 1420–1426.
[18] X. Qiu, Microstructure, hardness and corrosion resistance of $Al_2CoCrCuFeNiTix$ high-entropy alloy coatings prepared by rapid solidification, J. Alloys Compd. 735 (2018) 359–364.
[19] S. Sheikh, M.K. Bijaksana, A. Motallebzadeh, S. Shafeie, A. Lozinko, Lu. Gan, T. Tsao, U. Klement, D. Canadinc, H. Murakami, S. Guo, Accelerated oxidation in ductile refractory high-entropy alloys, Intermetallics 97 (2018) 58–66.
[20] S.V. Dhandapani, E. Thangavel, M. Arumugam, K.S. Shin, V. Veeraraghavan, S.Y. Yau, C. Kim, D.E. Kim, Effect of Ag content on the microstructure, tribological and corrosion properties of amorphous carbon coatings on 316L SS, Surf. Coat. Technol. 240 (2014) 128–136.
[21] Y. Shi, L. Collins, N. Balke, P.K. Liaw, B. Yang, In-situ electrochemical-AFM study of localized corrosion of $Al_xCoCrFeNi$ high-entropy alloys in chloride solution, Appl. Surf. Sci. 439 (2018) 533–544.
[22] R. Mishra, R. Balasubramaniam, Effect of nanocrystalline grain size on the electrochemical and corrosion behavior of nickel, Corros. Sci. 46 (2004) 3019–3029.
[23] M. Zhu, C. Du, X. Li, Z. Liu, S. Wang, J. Li, D. Zhang, Effect of AC current density on stress corrosion cracking behavior of X80 pipeline steel in high pH carbonate/bicarbonate solution, Electrochim. Acta 117 (2014) 351–359.
[24] D.D. Macdonald, The history of the point defect model for the passive state: a brief review of film growth aspects, Electrochim. Acta 56 (2011) 1761–1772.
[25] F. Borgioli, E. Galvanetto, T. Bacci, Corrosion behaviour of low temperature nitrided nickel-free, AISI 200 and AISI 300 series austenitic stainless steels in NaCl solution, Corros. Sci. 136 (2018) 352–365.
[26] C.E.B. Marino, L.H. Mascaro, EIS characterization of a Ti-dental implant in artificial saliva media: dissolution process of the oxide barrier, J. Electroanal. Chem. 568 (2004) 115–120.
[27] H. Luo, Z. Li, A.M. Mingers, D. Raabe, Corrosion behavior of an equiatomic CoCrFeMnNi high-entropy alloy compared with 304 stainless steel in sulfuric acid solution, Corros. Sci. 134 (2018) 131–139.
[28] X. Cheng, Y.J. Huang, B.J. Zhou, P. Xue, H.B. Fan, J.F. S, Electrochemical and XPS studies of a Nb-containing Ti-based glass-forming alloy system in H_2SO_4 solution, Electrochem. Commun. 60 (2015) 139–143.
[29] I. Milošev, G. Žerjav, J.M.C. Moreno, M. Popa, Electrochemical properties, chemical composition and thickness of passive film formed on novel Ti–20Nb–10Zr–5Ta alloy, Electrochim. Acta 99 (2013) 176–189.
[30] S. Ningshen, M. Sakairi, K. Suzuki, T. Okuno, S. Ningshen, M. Sakairi, K. Suzuki, et al., Corrosion performance and surface analysis of Ti–Ni–Pd–Ru–Cr alloy in nitric acid solution, Corros. Sci. 91 (2015) 120–128.
[31] A.I. Karayan, S. Park, K. Lee, Corrosion behavior of Ti–Ta–Nb alloys in simulated physiological media, Mater. Lett. 62 (2008) 1843–1845.
[32] C.C. Shih, C.M. Shih, K.Y. Chou, S. Lin, Y. Su, Electrochemical behavior of $MP_{35}N$ implant alloy in simulated physiological media, J. Electrochem. Soc. 153 (10) (2006) B403–B410.
[33] C. Vasilescu, S.I. Drob, J.M.C. Moreno, P. Osiceanu, M. Popa, E. Vasilescu, M. Marcu, P. Drob, Long-term corrosion resistance of new Ti–Ta–Zr alloy in simulated physiological fluids by electrochemical and surface analysis methods, Corros. Sci. 93 (2015) 310–323.
[34] J. Lin, S. Ozan, K. Munir, K. Wang, X. Tong, Y. Li, C. Wen, Effects of solution treatment and aging on the microstructure, mechanical properties, and corrosion resistance of a β type Ti–Ta–Hf–Zr alloy, RSC Adv. 7 (2017) 12309–12317.
[35] Y. Qiu, M.A. Gibson, H.L. Fraser, N. Birbilis, Corrosion characteristics of high entropy alloys, Mater. Sci. Technol. 31 (2015) 1235–1243.
[36] A. Pardo, M.C. Merino, A.E. Coy, F. Viejo, R. Arrabal, E. Matykina, Pitting corrosion behaviour of austenitic stainless steels–combining effects of Mn and Mo additions, Corros. Sci. 50 (2008) 1796–1806.